ACS OMEGA

Open Access

http://pubs.acs.org/journal/acsodf

Article

Study of the Influence of Electron Spin in Ferromagnetism and Thermoelectric Characteristics of $CdTm_2Y_4$ (Y = S, Se) Spinels for Spintronic Applications

Huda A. Alburaih, Sadia Nazir,* Naveed Ahmed Noor,* Amel Laref, and Ramesh Sharma

Cite This: *ACS Omega* 2023, 8, 40341−40350

Read Online

ACCESS | Metrics & More | Article Recommendations

ABSTRACT: The current study used full-potential methods to examine the ferromagnetic characteristics of $CdTm_2Y_4$(Y= S, Se) spinels; i.e., structural, elastic, electronic, and thermoelectric characteristics of these spinels have been explored for the first time. We used PBEsol-GGA for enthalpy of formation calculations to explain the stability of the ferromagnetic state and calculate the elastic constants and corresponding mechanical modules to reveal the ductile behavior of the materials. The mBJ potential is used instead of PBEsol-GGA to obtain more accurate and precise results of electronic and thermoelectric characteristics. Using mBJ potential leads to complete occupation of the bands in the materials and a clear interpretation of the density of states (DOS). The analysis of the electronic band structure and DOS reveals the stability of the ferromagnetic state in the analyzed materials as a result of p−d hybridization-based exchange splitting of Tm cations in the lattice. The calculations of thermoelectric efficiency are effective in evaluating the aptitude pertinence of the material in waste energy recovery systems and other technological applications. The thermal parameters of these materials are also analyzed to examine their thermal stability over a wide range of temperatures. The results of these calculations are essential for determining the suitability of the materials for use in spintronics-based devices and thermoelectric appliances as these devices rely heavily on the material's thermoelectric properties.

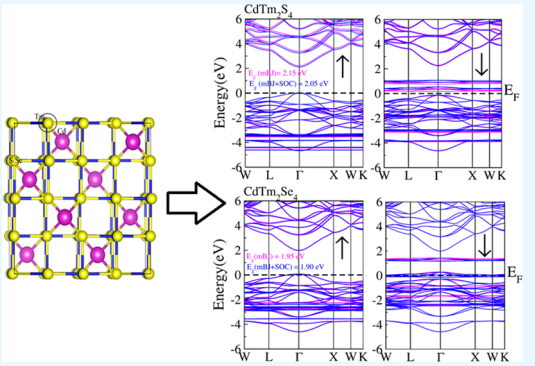

1. INTRODUCTION

The innovation of ferromagnetism, particularly chromium spinels and europium chalcogenides, around a half-century ago was expected[1] as insulators usually exhibit ferromagnetic or antiferromagnetic spin ordering steered through superexchange interaction; on the other hand, ferromagnetism was believed to be a property unique to metals. However, the Goodenough−Kanamori−Anderson imperatives guide cases where the superexchange interaction can result in ferromagnetic short-range coupling among confined spins. This mechanism is responsible for the Curie temperature T_C of 130 K in $CdCr_2Se_4$.[2,2] EuO and EuS are magnetic materials exhibiting antiferromagnetic order due to superexchange interactions between adjacent Eu^{2+} ions. This superexchange is overreacted by the direct ferromagnetic exchange between the f-electrons of one Eu^{2+} ion and the d-electrons of a neighbor, resulting in a net ferromagnetic interaction. In EuO, the ferromagnetic exchange interaction is stronger than in EuS, leading to a higher T_C of 68 K compared to 16 K in EuS.[3] Magnetic semiconductors are used for magneto-optical effects and colossal magneto-resistance. These properties arise due to the magnetic moments of the localized electron (f-electrons) interaction with the magnetic moments of itinerant electrons (band carriers). The coupling between f-electrons and band carriers also leads to fluctuations in the magnetization of the material near the Curie temperature.[4,5]

By introducing electron doping in the form of oxygen vacancies or by substituting Eu ions with Gd ions, the magnitude of T_C in EuO can be increased by about 50 K in agreement with the Ruderman−Kittel−Kasuya−Yasida (RKKY) theory. Recently, there have been proposals to utilize EuS and similar ferromagnetic insulators' functional overlayers, which can induce novel topological properties through the ferromagnetic proximity effect, particularly through the exchange splitting of interfacial bands.[6] On the other hand, $HgCr_2Se_4$, which has a Curie temperature T_C of 110 K, has been identified as a Weyl semimetal.[7] Rare-earth pyrochlores with the composition $Ln_2Ti_2O_7$ have been the subject of extensive study due to their intriguing magnetic behavior. The magnetic properties of these compounds can be altered over a broad range by carefully tuning the balance between various

Received: June 30, 2023
Accepted: October 6, 2023
Published: October 20, 2023

factors, including single-ion anisotropy, dipole interactions, and exchange couplings.[8−12]

One key feature of many rare-earth pyrochlores is the generation of highly anisotropic spin states, which arises from the strong crystal field experienced by the rare-earth ions within the pyrochlore lattice. In compounds such as $Dy_2Ti_2O_7$ and $Ho_2Ti_2O_7$, the specific ferromagnetic coupling and spin directions are crucial in generating spin ice properties. These materials exhibit spin orientations that resemble the position of hydrogen atoms in water ice, giving rise to a spin ice-like behavior.[13−19] This similarity has attracted significant attention in the study of transition-metal-based spinels like $CdFe_2O_4$ and $ZnCr_2O_4$ due to their geometric frustration.[20,21] Still, the existence of relatively potent spin−lattice couplings within the transition-metal-based materials is frequently directed to a decisive state in which structural transitions and magnetic ordering are coupled.[22,23] $CdLn_2S_4$ (Ln = Ho, Er, Tm, Yb) and $CdLn_2S_4$ (Ln = Dy, Ho) have been registered as suitable semiconductors with band gap equal to or greater than 2 eV according to available experimental data.[24,25]

In these spinels, the cationic distribution and arrangement contribute to the formation of magnetic sublattices resembling pyrochlores. An appropriate choice of exchange-correlation functional is critical in density functional theory (DFT) calculations to probe magnetically frustrated structures[26] accurately. The manipulation of magnetic materials has found many potential applications in various fields, such as giant-magneto-resistance (GMR) and tunnel-magneto-resistance (TMR), which are utilized in magnetic sensors and storage devices.[27,28] Past theoretical studies on magnetic materials such as $CdTm_2Y_4$ (Y = S, Se) have revealed that using the standard exchange-correlation functional is not appropriate for precisely exploring structural characteristics.[29] This present investigation on the magnetic semiconductors $CdTm_2Y_4$ (Y = S, Se) and the use of a superior exchange-correlation functional (ECE) can accurately probe their electronic and transport properties. A magnetic semiconductor is a material for which the Fermi level falls in the middle of the band gap for both spin-up and spin-down, while the half-metallic semiconductor has only one set of bands where the Fermi level falls in the middle of the band gap.[30,31] Theoretical investigations of chalcogenide spinel compounds such as $CdTm_2Y_4$ (Y = S, Se) have received relatively less attention (only electronic properties) in the available literature.[32] Therefore, the present study fills a gap in knowledge by examining the magnetic, electronic, and thermoelectric characteristics of these materials using the Wien2k code with the FP-LAPW + lo method.[33] Since the electronic properties computed in the present work are calculated using the TB-mBJ functional, the electronic structures for the valence electrons (including the f-electrons of Tm) are reliably computed in the present work. The thermoelectric properties computed in the present work show that the magnetic state of the studied materials can be advantageous for realizing improved transport properties that can in turn be useful for spintronic applications. This investigation is an important step toward exploring theoretical and experimental investigations of these materials for potential technological applications such as spintronics.

2. COMPUTATIONAL DETAILS

The TB-mBJ potential is a modified form of the traditional DFT exchange-correlation functional that has been shown to give more accurate electronic structural calculations for materials with localized states as that of the experimental study and has been applied with full-potential-linearized augmented plane wave + lo method in the Wien2k package program to explore the electronic and magnetic characteristics of $CdTm_2Y_4$ (Y = S, Se).[34−36] The mathematical expressions for the TB-mBJ potential functional are as follows

$$V_{x,\sigma}^{\text{TB-mBJ}}(r) = cV_{x,\sigma}^{\text{BR}}(r) + (3c - 2)\frac{1\sqrt{5}\sqrt{2t_\sigma(r)}}{\pi 12\rho_\sigma(r)} \quad (1)$$

where C and $\rho(r)$ represent the charge convergence and density and $V_{x,\sigma}^{\text{BR}}$ is Becke−Roussel potential the "C" is expressed as

$$c = \alpha + \left(\beta\frac{1}{V_{\text{cell}}}\int d^3r\frac{|\nabla\rho(r)|}{\rho(r)}\right)^{1/2} \quad (2)$$

The Trans-Bhalla improved Becke−Johnson (TB-mBJ) functional is known for accurately reproducing experimental band gaps of materials. TB-mBJ was employed in this study, which allows for a computationally efficient method to calculate electronic characteristics using a hybrid approach combining density functional theory (DFT) and the GM approximation. Additionally, we also include the spin−orbital coupling (SOC) to the TB-mBJ potential for more precise calculations of electronic properties. The linear-augmented-plane-wave (LAPW) method has been used as a basis set in the study, with a partition made in unit cells to nonoverlapping muffin-tin (MT) regions and the interstitial region. This approach ensures that the wave function behaves automatically inside the muffin-tin region and wave-like in the interstitial regions, providing an accurate representation of the material's electronic structure. This computational approach calculates the materials' electronic properties, including the band gap and energy eigenvalue for magnetic particle systems.

The product of R_{MT} and K_{max} is taken at 8, where R_{MT} represents the smallest muffin-tin radius and k_{max} is the maximum value of the reciprocal lattice. The 1000 k-points are used for reciprocal-space sampling. This means that calculations involving the band structure and optical characteristics are performed at these 1000 specific k-points in the Brillouin zone. Consecutive repetitions of the self-consistent field (SCF) of computation are performed likely until both the energy convergence (0.0001 Ry) and charge convergence (0.00001e) criteria are satisfied. Additionally, BoltzTrap program package is used for precise calculations of electronic transport properties and thermoelectric properties.[37] The following expressions are used to calculate the electrical conductivity

$$\sigma_{\alpha\beta}(\varepsilon) = \frac{1}{N}\sum_{i,k}\sigma_{\alpha\beta}(i,k)\frac{\delta(\varepsilon - \varepsilon_{i,k})}{\delta(\varepsilon)} \quad (3)$$

$$\sigma_{\alpha\beta}(i,k) = e^2\tau_{i,k}v_\alpha(i,\vec{k})v_\beta(i,\vec{k}) \quad (4)$$

Also, S and σ were calculated using T and μ

$$\sigma_{\alpha\beta}(\alpha,\mu) = \frac{1}{\Omega}\int\sigma_{\alpha\beta}(\varepsilon)\left[-\frac{\delta f_0(T,\varepsilon,\mu)}{\delta\varepsilon}\right]d\varepsilon \quad (5)$$

https://doi.org/10.1021/acsomega.3c04161
ACS Omega 2023, 8, 40341−40350

$$S_{\alpha\beta}(T,\mu) = \frac{1}{eT\Omega\sigma_{\alpha\beta}(T,\mu)} \int \sigma_{\alpha\beta}(\varepsilon)(\varepsilon-\mu)\left[-\frac{\delta f_0(T,\varepsilon,\mu)}{\delta\varepsilon}\right]d\varepsilon \quad (6)$$

Equations 5 and 6 are used to calculate the Seebeck coefficient and electrical conductivity. The BoltzTraP software assumes insignificance of phonon impact on thermal conductivity (κ_l), leading to the utilization of Slack's model[38] for computation. Based on this framework, κ_l can be evaluated using the subsequent expression

$$\kappa l = B\frac{M\theta_\alpha^3\delta V^{1/3}N}{\gamma^2 T} \quad (7)$$

The constant $B = 5.72 \times 10^{-8} \times 0.849/2(1-0.514/\gamma + 0.228/\gamma^2)$ is defined as a fixed value. M denotes the average atomic mass, δ is the cubic root of the average atom volume, Θ_D stands for the acoustic Debye temperature, n signifies the atoms per unit cell count, and γ indicates an acoustic Gruneisen constant. The Debye temperature defines the crystal's vibrational spectrum, while the Gruneisen constant gauges the degree of lattice anharmonicity in a material. This equation has found extensive application in k-calculations.[39−41] The computed κ_l values for the given material within the temperature range of 100−1200 K have been illustrated in the figure, demonstrating a declining trend in κ with increasing temperature

3. RESULTS AND DISCUSSION

3.1. Structural and Mechanical Stability. The structural characteristics of $CdTm_2Y_4$ (Y = S, Se) compounds have been performed. The unit cell structures of these compounds, which belong to the spinel crystal structure, have been obtained using the structural generated function implemented in Wien2K code[33] and shown in Figure 1. The spinel structure is described by the $Fd\bar{3}m$ (227) space group.[42] The atomic positions are specified in $CdTm_2Y_4$ (Y = S, Se) as follows: Cd is located at the atomic position (0.125, 0.125, 0.125), Tm is at position (0.5, 0, 0), and S is found at (0.25, 0.25, 0.25) within the unit cell.

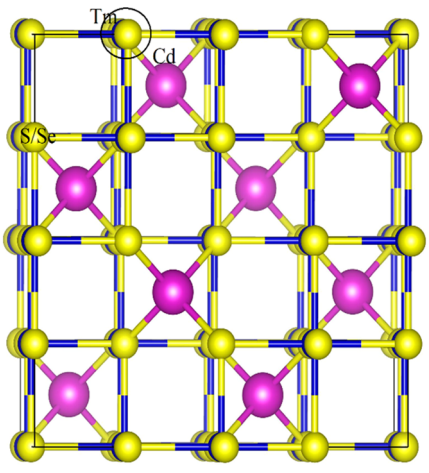

Figure 1. Rare-earth-based crystal structure of $CdTm_2Y_4$ (Y = S, Se). Orange, blue, and yellow spheres represent Cd, Tm, and Y atoms.

The bulk moduli (B) and the lattice parameters of $CdTm_2Y_4$ (Y = S, Se) compounds were then optimized using the Murnaghan equation[43] and fitting the computed volumes and energies, and these optimized values are presented in Table 1.

Table 1. Calculated Lattice Constant, Bulk Modulus, Energy Differences (ΔE_1 (eV) and ΔE_2 (eV)), Formation Energy, Elastic Constant, Shear Modulus, Young's Modulus, Pugh's Ratio, Poisson's Ratio, and Anisotropy Factor for Cubic $CdTm_2Y_4$ (Y = S, Se)

	$CdTm_2S_4$		$CdTm_2Se_4$	
parameters	PBEsol-GGA	exp.	PBEsol-GGA	exp.
a_o (Å)	11.04	11.10[a]	11.54	11.56[b]
B_o (GPa)	68.21		54.35	
ΔE_1 (eV)	28.33		19.26	
ΔE_2 (eV)	6.84		4.96	
ΔH_f (eV)	−2.46		−1.93	-
$\uparrow E_g$ (eV)	2.15		1.95	
C_{11} (GPa)	112.66		94.31	
C_{12} (GPa)	42.74		30.15	
C_{44} (GPa)	74.66		34.44	
B (GPa)	66.04		51.53	
G (GPa)	55.59		33.47	
Y (GPa)	129.26		82.55	
B/G	1.19		1.54	
υ	0.17		0.23	
A	2.135		1.07	

[a]Ref 44. [b]Ref 45.

A material's hardness is related to its bulk modulus B under an applied pressure. The computer values of lattice parameters (a (Å)) and bulk moduli for $CdTm_2Y_4$ (Y = S, Se) compounds differ from the values reported in the existing experimental and theoretical literature, suggesting the accuracy of the computed results.[44,45,29] The obtained results indicate that the replacement of "Se" with "S" decreases B and increases a (Å).

This inverse relation between "B" and "a (Å)" is consistent with the behavior expected in the crystal structure. When larger ions (in this case, S^{2+} ions with a larger ionic radius of 0.80 Å) replace smaller ones (Se^{2+} ions with a smaller ionic radius of 0.74 Å), it causes an expansion of the host lattice. This expansion results in an increased lattice constant a[46] and reduces the crystal lattice's stiffness, leading to a decrease in the bulk modulus (B). The decrease in B indicates that the material becomes more susceptible to deformations caused by the applied pressure. The enthalpy of formation (ΔH_f) for the spinel compounds is expressed as

$$(\Delta H_f) = E_{tot}(Cd_lTm_mY_n) - lE_{cd} - mE_{Tm} - nE_Y \quad (8)$$

Here, E_{tot} ($Cd_lTm_mY_n$) is used as the ground-state energy, while E_{Cd}, E_{Tm}, and E_Y represent the individual atom ground-state energies. The letters l, m, and n represent the number of atoms per unit cell of cadmium, thulium, and sulfur/selenium, respectively. The negative value of ΔH_f for the studied spinels (see Table 1) indicates that these spinels are thermodynamically stable and further confirms the stability of the ferromagnetic phase over the paramagnetic phase. This is because the (ΔH_f) values are obtained for the spinel compound's specific crystal structure and magnetic state. Table 1 represents the positive value of total energy difference (ΔE_1 and ΔE_2) obtained from $\Delta E_1 = E_{NM} - E_{FM}$ and $\Delta E_2 = E_{AFM} - E_{FM}$, where E_{NM}, E_{AFM}, and E_{FM} represent the total

https://doi.org/10.1021/acsomega.3c04161
ACS Omega 2023, 8, 40341−40350

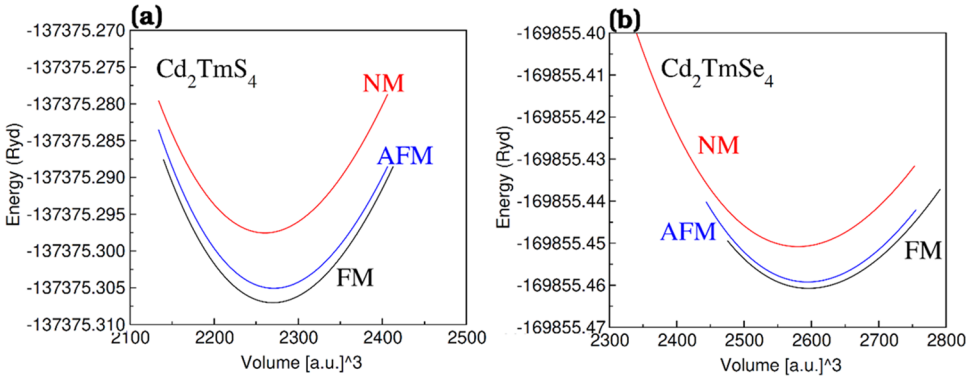

Figure 2. Volume optimization versus energy plots for (a) $CdTm_2S_4$ and (b) $CdTm_2Se_4$ compounds in ferromagnetic (FM), antiferromagnetic (AFM), and nonmagnetic (NM) phases.

energies of the nonmagnetic, antiferromagnetic, and ferromagnetic states, respectively, providing clear evidence that the ferromagnetic conditions are more stable compared to nonmagnetic and antiferromagnetic states in the spinel compounds under investigation (see Figure 2).

The Charpin method is used for the values of $CdTm_2Y_4$ (Y = S, Se), elastic constants (C_{11}, C_{12}, and C_{44}), and other related parameters.[33] By substituting the values of elastic constants obtained from the Charpin method in the given equations,[47−53] the values of various parameters (bulk modulus *B*, Young's modulus *E*, shear modulus *G*, and anisotropy factor (A)) and Poisson's ratio (υ) for the Pugh ratio (B/G) for the cubic spinels $CdTm_2S_4$ or $CdTm_2Se_4$ have been evaluated

$$B = \frac{1}{3}(C_{11} + 2C_{12}) \tag{9}$$

$$G = \frac{1}{2}(G_V + G_R) \tag{10}$$

where

$$G_R = \frac{5C_{44}(C_{11} - C_{12})}{4C_{44} + 3(C_{11} - C_{12})}$$

$$G_v = \frac{1}{5}(C_{11} - C_{12} + 3C_{44})$$

and

$$E = \frac{9BG}{3B + G} \tag{11}$$

$$A = \frac{2C_{44}}{(C_{11} - C_{12})} \tag{12}$$

$$\nu = \frac{3B - 2G}{2(3B + G)} \tag{13}$$

It is indeed important to ensure that the calculated elastic constants satisfy certain conditions to probe the elastic stability of the material as $1/3(C_{11} + 2C_{12}) > 0$; $C_{44} > 0$; $1/2\ (C_{11} - C_{12}) > 0$ and $C_{12} < B < C_{11}$. These conditions are based on the physical requirements that the elastic constant must satisfy for the material to be mechanically stable and not undergo elastic instability. Based on the results of the computations for elastic constants of spinels $CdTm_2Y_4$ (Y = S, Se) and the application of the abovementioned condition reveals that both spinels are elastically stable.

The values of elastic constants are used in eq 8 to obtain the bulk modulus and are shown in Table 1. The spinel structure's bulk modulus decreases when S is substituted with Se. This decreasing trend in the bulk modulus is consistent with the results obtained from energy minimization, as shown in Table 1. The elastic anisotropy factor (A) is a measure of the degree of anisotropy in the crystal structure. Based on the computed value presented in Table 1 using eq 11 reveals that the studied spinels $CdTm_2S_4$ or $CdTm_2Se_4$ exhibit considerable deviation from unity for the anisotropic elastic factor (A). Young's modulus measures a material's stiffness or resistance to deformation when subjected to external pressure or stress along a specific axis. The computed value of *E* using eq 10 is presented in Table 1. Young's modulus decreases noticeably when S is replaced with Se in the spinel structure. This decrease in *E* suggests that the studied spinels $CdTm_2S_4$ or $CdTm_2Se_4$ exhibited lower deformation stiffness than $CdTm_2S_4$.

The shear modulus quantifies the material's ability to withstand shear stresses without undergoing plastic deformation. The calculated value of "*G*′′ is shown in Table 1 by using eq 9. The value of "*G*′′ is decreased from 55.59 to 33.47 GPa by replacing S with Se. These computed values suggest a lower resistance to shear deformation for $CdTm_2Se_4$ as compared to $CdTm_2S_4$. The Poisson's ratio (υ) and Pugh ratio (B/G) are used to interpret materials brittleness or ductility. Poisson's ratio is obtained by using eq 13, and eq 9 is used for Pugh ratio. The values of υ and (B/G) for $CdTm_2S_4$ and $CdTm_2Se_4$ as presented in Table 1 are less than the critical values of 0.26 and 1.75, respectively, which suggests that both materials are ductile. This makes them potentially useful for mechanical device applications that require materials with good deformability and toughness.

3.2. Electronic and Magnetic Properties. The electronic structure of a material plays a crucial role in determining the properties and potential applications in various electronic devices. The energy gap is a key parameter for memory, smart, and spintronics device applications, as it governs the material's efficiency and functionality in these devices. The energy gap allows for controlling the flow of charge and spin in electronic devices, enabling information storage, processing, and manipulation functions. The energy gap and spin-polarized band structure of the cubic FM phase of $CdTm_2Y_4$ (Y = S, Se) were calculated using the ground-state value of the lattice constant.

https://doi.org/10.1021/acsomega.3c04161
ACS Omega 2023, 8, 40341−40350

To accurately capture the electronics features of $CdTm_2Y_4$ (Y = S, Se) compounds, Trans-Bhala improved Becke−Johnson (TB-mBJ) potential is applied. Additionally, TB-mBJ potential plus spin orbital coupling (SOC) are used that provides a more precise description of the electronic structure (see Figure 3). The spin-polarized band structure of the spinel

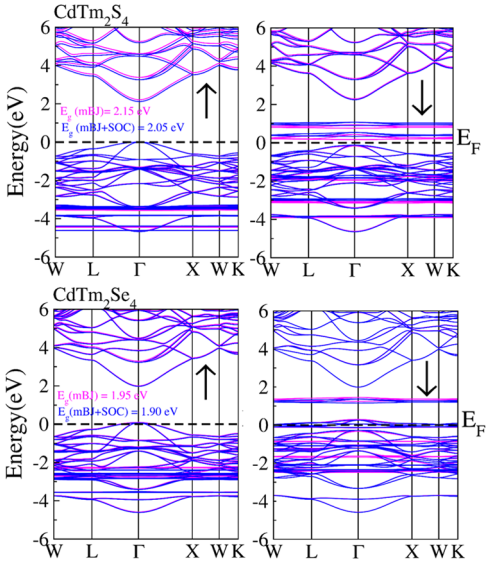

Figure 3. Electronic band structures computed for $CdTm_2S_4$ and $CdTm_2Se_4$ for majority and minority spin channels using the mBJ and mBJ + SOC potential.

compounds $CdTm_2Y_4$ (Y = S, Se) and the computation of the direct band gap values at the Γ-point of the first Brillouin zone using the spin-up band structure have been noticed. The calculated values of direct band gap $E_g(\Gamma-\Gamma)$ considering the spin-up band structure are presented in Table 1 for $CdTm_2Y_4$ (Y = S, Se). Figures 4 and 5 illustrate the density of states, providing valuable insights into the electronic structure of the spinel compounds $CdTm_2Y_4$.

The TDOS represents the overall distribution of the electron state, while PDOS shows the contribution of different atoms and atomic levels to the band structure. The existence of Tm atoms in the lattice introduces splitting effects, resulting in the lifting of the valence band maximum (VBM) related to spin-up carriers toward the Fermi level. This indicates that the spin-up electrons have a higher probability of occupying states closer to the Fermi level. Conversely, the conduction band minimum (CBM) is shifted away from the Fermi level toward higher energy for spin-up carriers, indicating that it requires more energy for spin-up electrons to transition into the conduction band. On the other hand, the trend observed for spin-down carriers is converse to that of spin-up carriers, as shown in Figure 3.

The absence of energy states at the Fermi level indicates that both $CdTm_2Y_4$ (Y = S, Se) compounds exhibit a semiconducting nature rather than the half-metallic nature and suggests that there is no complete spin polarization and both spin channels contribute to the electronic states. The PDOS analysis, as depicted in Figures 4 and 5, provides insights into the ferromagnetism and exchange mechanism in the compounds. In the spin-up channel, 4f states of Tm atoms are observed in the energy range of −2.8 to −4.6 eV. Similarly, hybridization occurs between the 2p states of S/Se atoms and Cd states in the energy range of 0 to −2.0 eV. These hybridization phenomena in the spin-up channel contribute to the materials' overall electronic structure and magnetic properties.

Furthermore, hybridization between the 4f states of Tm atoms and 2p states of S/Se atoms within the conduction band is detected in the energy range of 3−5.0 eV for the spin-down channel as well as for the spin-up channel for the same energy range. These hybridization effects contribute to the materials' overall electronic properties and exchange mechanisms.

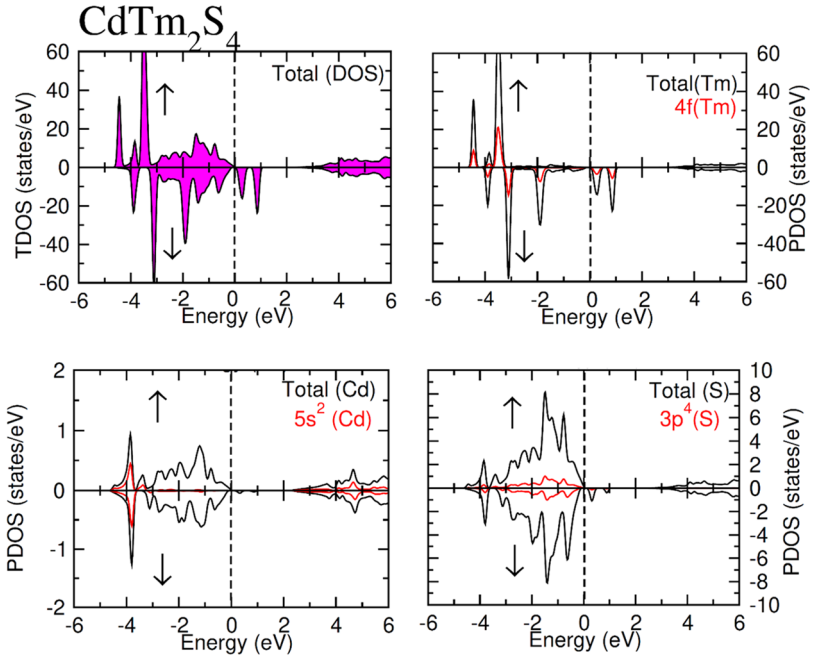

Figure 4. Total density of states of $CdTm_2S_4$ spinel and their partial density of states of Cd, Tm, and S atoms with respect to spin-up (↑) and spin-down (↓) channels.

https://doi.org/10.1021/acsomega.3c04161
ACS Omega 2023, 8, 40341−40350

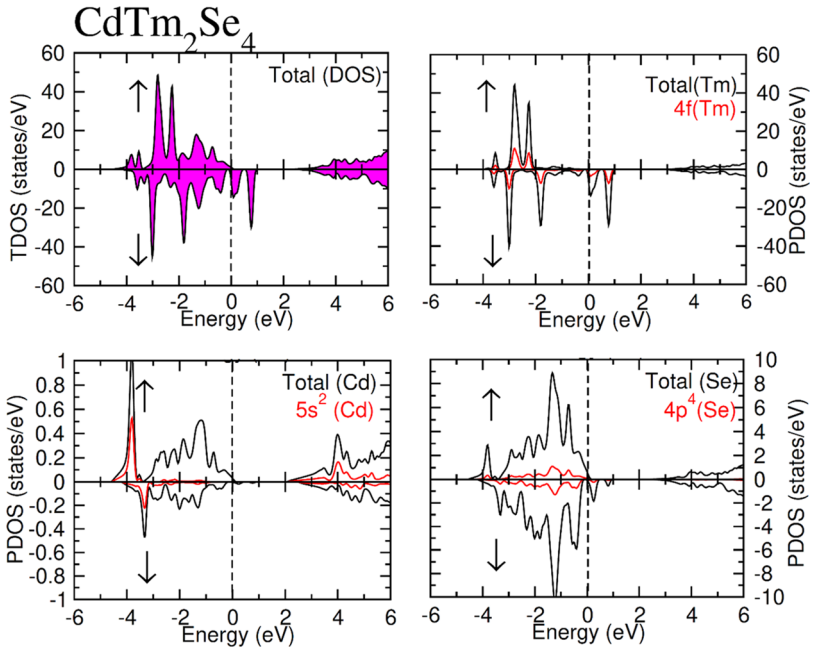

Figure 5. Total density of states plot for the $CdTm_2Se_4$ spinel along with their partial density of states plots of Cd, Tm, and Se atoms with respect to spin-up (↑) and spin-down (↓) channels.

The computed magnetic moment (μ_T) for both spinel compounds $CdTm_2Y_4$ (Y = S, Se) is 4 μ_B. This total magnetic moment is mainly contributed by the Tm atom, indicating that Tm plays a significant role in the overall magnetism of the compounds. On the other hand, the contribution of Cd and Y atoms to the total magnetic moment is relatively low. The contribution of different atoms toward the total magnetic moment is also calculated and presented in Table 2. The

Table 2. Total Magnetic Moments and Local Magnetic Moments (in Terms of μ_B) for $CdTm_2S_4$ and $CdTm_2Se_4$

	total	int.	Cd	Tm	S/Se
$CdTm_2S_4$	4.000	0.0992	0.0018	1.8829	0.0457
$CdTm_2Se_4$	4.000	0.1411	0.0036	1.7152	0.0992

electronic bonding interactions between their rare-earth (RE) dopant atoms and the host lattice atoms lead to variations in the valency of Tm and, ultimately, research in a ferromagnetic (FM) stable state of the compound. The strong coupling between the p state of the S/Se atom and the f state of the Tm atom results in the creation of magnetic moments.

The value of the interstitial magnetic moment of the rare-earth atom is the same as the total magnetic moment, revealing that the strong ferromagnetic exchange splitting induces magnetic effects, effectively converting the Tm atom into a magnetic atom. The magnetic moment of S/Se and Cd atoms is also calculated and attributed to their FM coupling with Tm atoms.

3.3. Thermoelectric Properties. Indeed, converting waste heat into electrical energy is a promising approach to address the increasing demand for electrical power while utilizing existing heat sources. Thermoelectric materials play a vital role in converting heat directly into electricity. Worldwide are actively engaged in intensive research to discover novel and efficient thermoelectric materials that can meet these energy demands.[54,55] Among the various materials being investigated, spinel chalcogens have shown great promise as potential thermoelectric materials.

These materials are particularly attractive for thermoelectric applications due to their small band gap.[56,57] In this study, two such chalcogen materials, $CdTm_2Y_4$ and $CdTm_2$, have been examined. The band gap reduction observed by replacing S with Se indicates an improvement in their efficiency for thermoelectric uses. The investigation of important thermoelectric parameters, including the electrical conductivity σ, Seebeck coefficient, power factors electronic and phononic part of thermal conductivity, and figure of merit (ZT), has been carried out over a wide temperature range from 0 to 800 K and presented in Figures 6(a−c) and 7(a−c). It is worth noting that calculating these thermoelectric properties involves certain conditions during this study. The constant relaxation time approximation is applied, which assumes a fixed relaxation time for the charge carrier. As a result, the computed values of electrical and thermal conductivities are presented in units of $(\Omega.m.s)^{-1}$ and (W/Kms), respectively. To compare the computed results with the experimental values, the calculated values must be multiplied by the observed relaxation time.[58,59] All of the TE calculations were carried out using the semiclassical BTE within the constant relaxation time (10^{-14} s) approximation, as implemented in the BoltzTrap code. This approximation is based on the assumption that the scattering time does not vary strongly with energy. Note that such an approximation has been successfully used in the past to predict the thermoelectric properties of materials.[60,61]

The electrical conductivity represented by σ/τ (where "τ" is the relaxation time) is associated with flow of charge carriers indicating the forward current. At temperatures of 300 and 800 K, the electrical conductivities of $CdTm_2S_4$ and $CdTm_2Se_4$ and are reported as 2.0, 11.1 ($\times 10^4\ \Omega^{-1}\ m^{-1}$), and 7.5, 17.5 ($\times 10^4\ \Omega^{-1}\ m^{-1}$), respectively. This indicates an increase in "σ" with temperature (see Figure 6(a)). Having a high electrical conductivity at room temperature is a key feature of thermoelectrically useful materials. The studied compounds

https://doi.org/10.1021/acsomega.3c04161
ACS Omega 2023, 8, 40341−40350

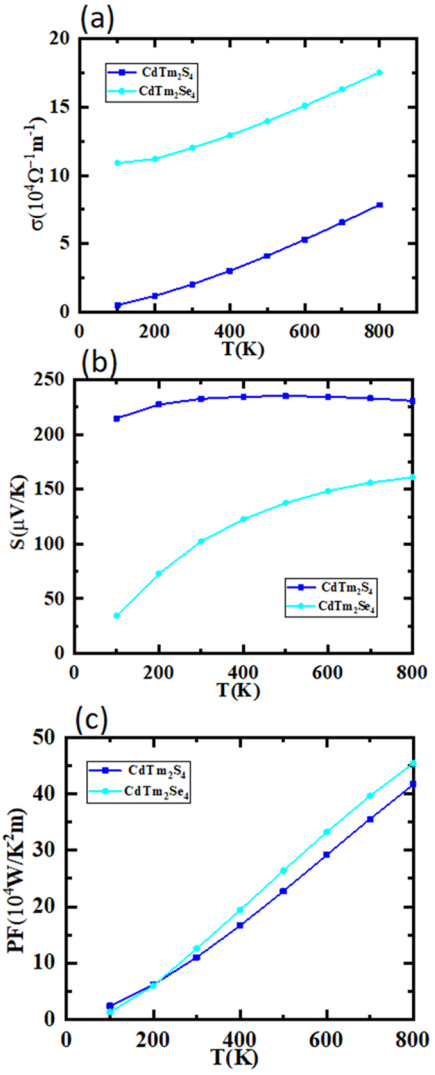

Figure 6. Computed (a) electrical conductivity, (b) Seebeck coefficients (S), and (c) power factor (PF) against temperature for $CdTm_2S_4$ and $CdTm_2Se_4$ compounds.

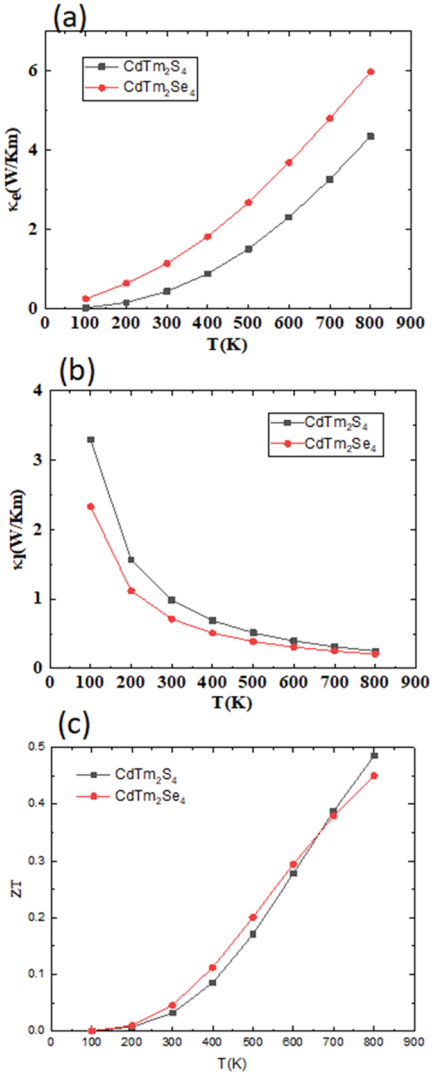

Figure 7. Computed (a) electronic (κ_e) thermal conductivity, (b) phononic (κ_l) thermal conductivity, and (c) figure of merit (ZT) against temperature for $CdTm_2S_4$ and $CdTm_2Se_4$ compounds.

are nondegenerate semiconductors; it is evident from the band structure that the calculated band gap values of $CdTm_2S_4$ and $CdTm_2Se_4$ compounds in spin-up channels are 2.04 and 1.90 eV, respectively. In contrast, spin-down channels indicate a small band gap, with a small amount of heat energy valence electron that can surmount this band gap, and the electronic states just above the Fermi energy level will get filled. Once these states get occupied, then there is no empty space for further thermally excited electrons. Because the energy bands just above the Fermi level in the conduction band show a flat behavior, it means the electrons have no conduction at all. In order for conduction to occur, an electron must be excited to the next available state, which is at the highest energy. Hence, at higher temperatures, these electrons will get further excited to the deep conduction band, and this is why these compounds behave like nondegenerate semiconductors. Thermoelectric materials possess a crucial characteristic of generating voltage through temperature gradients. This phenomenon is directly influenced by two significant parameters: Seebeck coefficient (S) and thermopower. Due to the high value of electrical conductivity, compromises are often necessary for achieving optimal performance in these materials. In our investigation of $CdTm_2S_4$ (see Figure 6(b)), the S value was measured as 100 μVK^{-1} at 300 K. As the temperature increased, the S value increased as up to 800 K. Interestingly, a distinct variation trend of "S" with temperature was observed in $CdTm_2Se_4$. The variations in the Seebeck coefficient with temperature have also been noticed in rare-earth Cd-based spinels such as $CdEr_2X_4$ (X = S, Se).[62]

The Seebeck coefficient is a time-independent parameter that makes it comparable to experimental data, providing valuable insights into the thermoelectric behavior of the materials. The power factor (PF = $S^2\sigma$) and figure of merit ($ZT = S^2\sigma T/k\epsilon$) are important parameters in assessing the thermoelectric performance of materials. The relaxation time independence of ZT makes it comparable to experimental data, further validating its usefulness in evaluating the efficiency of thermoelectric materials. The power factor (PF) is a parameter that measures the thermoelectric power generation of a material and depends on the value of the Seebeck coefficient (S) and electrical conductivity (σ). The PF values were calculated as 10 and 12 ($\times 10^4$ W/mK^2) at 300 K for $CdTm_2Y_4$ (Y = S, Se) compounds (see Figure 6c). As the temperature

https://doi.org/10.1021/acsomega.3c04161
ACS Omega 2023, 8, 40341−40350

increased to 900 K, the PF values correspondingly increased to 41 and 45 ($\times 10^4$ W/mK^2).

Fourier's law describes the heat flux in a thermoelectric material using the mathematical equation $q = -k\frac{dq}{dx}$. In this equation, "q" represents the rate of thermal energy flow per unit area over time, "k" denotes the coefficient of thermal conductivity, and $\frac{dq}{dx}$ represents the temperature gradient. Both phonons and electrons influence the overall thermal conductivity in semiconductors, whereas in metals, the contribution of phonons is negligible, i.e., less than 2%. Since the interaction between electrons and phonons has a significant impact on determining the transport characteristics, this coupling has been incorporated into the investigation of thermoelectric features within the spinels under study. For the analysis of thermal conductivity, two distinct approaches have been employed: electron-based and phonon-based methods, denoted as $\kappa_t = \kappa_e + \kappa_l$. In this expression, κ_e signifies the contribution arising from electron vibration, while κ_l represents the thermal conductivity associated with phonon vibration. This relationship is visualized in Figure 7(a,b), depicting the calculated thermal conductivities attributable to electronic (κ_e) and phononic (κ_l) mechanisms across the temperature range of 0−900 K. The thermal conductivities are represented by black and blue curves for κ_l and total or overall conductivity, both of which decrease with increasing temperature. On the other hand, the red curve corresponds to κ_e thermal conductivity, displaying an upward trend as temperature increases up to 900 K.

Both compounds show insulating behavior in spin-up channels and metallic behavior in spin-down channels. For better understanding, we plotted electronic thermal conductivity κ_e and lattice thermal conductivity κ_l separately. Now, it is demonstrated that κ_e is the dominated part as compared to κ_l. For example, at T = 800 K, κ_e = 4, and κ_l = 0.25 W/Km (refer to Figure 7a,b). In addition, κ_l is decreasing with increasing temperature, while κ_e shows increasing behavior fulfilling the Wiedemann−Franz law. For $CdTm_2Se_4$, the electrical conductivity is of the order of $10^4\ \Omega^{-1}\cdot m^{-1}$, which is extremely high but consistent with the band gap of our compound. For semiconductor and half-metallic compounds, the Wiedemann−Franz law is $\sigma k = LT$, where σ is the electrical conductivity, k is the electronic thermal conductivity, T is the temperature, and L denotes the Lorentz number. The carrier electrical and thermal conductivities appear to increase with an increase in the temperature and hence follow the Wiedemann−Franz law. The calculated values were then employed to evaluate the figure of merit (ZT) for $CdTm_2Y_4$ spinels. Figure 7c demonstrates the variation in ZT as a function of temperature. Both compounds exhibit an increasing trend of ZT with temperature. At 800 K, the ZT values were measured as 0.5 and 0.45 for $CdTm_2S_4$ and $CdTm_2Se_4$, respectively. These calculations justify the potential utilization of the investigated chalcogens $CdTm_2Y_4$ in thermoelectric device applications.

4. CONCLUSIONS

Probing of physical properties of $CdTm_2Y_4$ (Y = S, Se) compounds, extensive DFT-based studies were accomplished. The calculations consistently confirmed the stability of the ferromagnetic (FM) state for both compounds, which was also supported by the enthalpy of formation. Moreover, investigating the elastic properties provides further insight into the mechanical behavior of these compounds for device applications. The ferromagnetic behavior was corroborated by observing higher ground-state energy in the FM states compared to the nonmagnetic (NM) states. The computer values of lattice parameters (a (Å)) for $CdTm_2Y_4$ (Y = S, Se) compounds differ from the values reported in the existing experiment, suggesting the accuracy of the computed results. The spin-polarized band structure of the studied spinels and the computation of the direct band gap values at the Γ-point indicate that both spinels have potential solar cell applications. The interpretation of exchange interactions and hybridizations from the calculated density of states indicates electronic spin that plays a significant role in the ferromagnetism of these chalcogens. The materials exhibited semiconducting magnetic behavior characterized by multiple integral values of total magnetic moment equal to $4\mu_B$. The favorable Seebeck coefficient and power factor of $CdTm_2Y_4$ (Y = S, Se) at ambient temperatures highlight their potential in the fields of energy harvesting applications.

AUTHOR INFORMATION

Corresponding Authors

Sadia Nazir − *Department of Physics, University of Lahore, Lahore 54000, Pakistan*; Email: sadiamalik.chep@gmail.com

Naveed Ahmed Noor − *Department of Physics, Riphah International University, Lahore Campus, Lahore 54660, Pakistan*; orcid.org/0000-0001-8039-1424; Email: naveedcssp@gmail.com

Authors

Huda A. Alburaih − *Department of Physics, College of Science, Princess Nourah Bint Abdulrahman University, Riyadh 11671, Saudi Arabia*

Amel Laref − *Department of Physics and Astronomy, College of Science, King Saud University, Riyadh 11451, King Saudi Arabia*

Ramesh Sharma − *Department of Applied Science, Feroze Gandhi Institute of Engineering and Technology, Raebareli 229001 Uttar Pradesh, India*

Complete contact information is available at: https://pubs.acs.org/10.1021/acsomega.3c04161

Notes

The authors declare no competing financial interest.

ACKNOWLEDGMENTS

The authors express their gratitude to the Princess Nourah Bint Abdulrahman University Researchers Supporting Project (Grant No. PNURSP2023R70), Princess Nourah Bint Abdulrahman University, Riyadh, Saudi Arabia.

REFERENCES

(1) Methfessel, S.; Mattis, D. C. Magnetic Semiconductors. In *Encyclopedia of Physics / Handbuch der Physik*; Springer, 1968; Vol. *18*, pp 389−563.

(2) Baltzer, P. K.; Wojtowicz, P. J.; Robbins, M.; Lopatin, E. Exchange interactions in fer- romagnetic chromium chalcogenide spinels. *Phys. Rev.* **1966**, *151*, 367−377.

(3) Wachter, P. Europium chalcogenides: EuO, EuS, EuSe and EuTe. In *Handbook on the Physics and Chemistry of Rare Earth*; Gschneidner, K. A., Jr; Eyring, L., Eds.; Elsevier, 1979; pp 507−574.

https://doi.org/10.1021/acsomega.3c04161
ACS Omega 2023, 8, 40341−40350

(4) Kasuya, T.; Yanase, A. Anomalous trans- port phenomena in Eu-chalcogenide alloys. *Rev. Mod. Phys.* **1968**, *40*, 684−696.
(5) Nagaev, E. L. Colossal-magnetoresistance materials: manganites and conventional ferromagnetic semiconductors. *Phys. Rep.* **2001**, *346*, 387−531, DOI: 10.1016/S0370-1573(00)00111-3.
(6) Žutić, I.; Matos-Abiague; Scharf, B.; Dery, H.; Belashchenko, K. Proximitized materials. *Mater. Today* **2019**, *22*, 85−107.
(7) Xu, G.; Weng, H.; Wang, Z.; Dai, X.; Fang, K. Chern semimetal and the quantized anomalous Hall effect in HgCr2Se4. *Phys. Rev. Lett.* **2011**, *107*, No. 186806, DOI: 10.1103/physrevlett.107.186806.
(8) Champion, J. D. M.; Harris, M. J.; Holdsworth, P. C. W.; Wills, A. S.; Balakrishnan, G.; Bramwell, S. T.; Cizmar, E.; Fennell, T.; Gardner, J. S.; Lago, J.; McMorrow, D. F.; Orendac, M.; Orendacova, A.; McK, D.; Smith, R. I.; Telling, M. T. F.; Wildes, A. $Er_2Ti_2O_7$: Evidence of quantum order by disorder in a frustrated antiferro-magnet. *Phys. Rev. B* **2003**, *68*, No. 02040(R), DOI: 10.1103/PhysRevB.68.020401.
(9) Gingras, M. J. P.; Stager, C. V.; Raju, N. P.; Gaulin, B. D.; Greedan, J. E. Static critical behavior of the spin-freezing transition in the geometrically frustrated pyrochlore antiferromagnet $Y_2Mo_2O_7$. *Phys. Rev. Lett.* **1997**, *78*, 947−950, DOI: 10.1103/PhysRevLett.78.947.
(10) Aung, Y. L.; Ikesue, A.; Yasuhara, R.; Iwamoto, Y. Optical properties of improved Tb2Hf2O7 pyrochlore ceramics. *J. Alloys Compd.* **2020**, *822*, No. 153564.
(11) Panghal, A.; Kumar, Y.; Kulriya, P. K.; Shirage, P. M.; Singh, N. L. Structural assessment and irradiation response of La2Zr2O7 pyrochlore: impact of irradiation temperature and ion fluence. *J. Alloys Compd.* **2021**, *862*, No. 158556.
(12) Gardner, J. S.; Dunsiger, S. R.; Gaulin, B. D.; Gingras, M. J. P.; Greedan, J. E.; Kiefl, R. F.; Lumsden, M. D.; MacFarlane, W. A.; Raju, N. P.; Sonier, J. E.; Swainson, I.; Tun, Z. Cooperative paramagnetism in the geometrically frustrated pyrochlore antiferromagnet Tb2Ti2O7. *Phys. Rev. Lett.* **1999**, *82*, 1012−1015, DOI: 10.1103/PhysRevLett.82.1012.
(13) Bazuev, G. V.; Chupakhina, T. I.; Korolyov, A. V. Synthesis, characterization and magnetic properties of complex oxides Ln2Mn2/3Re4/3O7 (Ln= Er, Y) and Y2Zn2/3Re4/3O7. *J. Alloys Compd.* **2009**, *486*, 88−92.
(14) Bramwell, S. T.; Harris, M. J. Frustration in Ising-type spin models on the pyrochlore lattice. *J. Phys.: Condens. Matter* **1998**, *10*, L215−L220, DOI: 10.1088/0953-8984/10/14/002.
(15) Ramirez, A. P.; Hayashi, A.; Cava, R. J.; Siddharthan, R.; Shastry, B. S. Zero-point entropy in spin ice. *Nature* **1999**, *399*, 333−335, DOI: 10.1038/20619.
(16) Snyder, J.; Slusky, J. S.; Cava, R. J.; Schiffer, P. How 'spin ice'freezes. *Nature* **2001**, *413*, 48−51, DOI: 10.1038/35092516.
(17) Snyder, J.; Ueland, B. G.; Mizel, A.; Slusky, J. S.; Karunadasa, H.; Cava, R. J.; Schiffer, P. Quantum and thermal spin relaxation in the diluted spin ice Dy2−xMxTi2O7 (M= Lu, Y). *Phys. Rev. B* **2004**, *70*, No. 184431.
(18) Snyder, J.; Ueland, B. G.; Slusky, J. S.; Karunadasa, H.; Cava, R. J.; Schiffer, P. Low-temperature spin freezing in the Dy2Ti2O7 spin ice. *Phys. Rev. B* **2004**, *69*, No. 064414.
(19) Fukazawa, H.; Melko, R. G.; Higashinaka, R.; Maeno, Y.; Gingras, M. J. P. Magnetic anisotropy of the spin-ice compound $Dy_2Ti_2O_7$. *Phys. Rev. B* **2002**, *65*, No. 054410.
(20) Snyder, J.; Ueland, B. G.; Slusky, J. S.; Karunadasa, H.; Cava, R. J.; Mizel, A.; Schiffer, P. Quantum-Classical Reentrant Relaxation Crossover in Dy2Ti2O7 Spin Ice. *Phys. Rev. Lett.* **2003**, *91*, No. 107201.
(21) Martinho, H.; Moreno, N. O.; Sanjurjo, J. A.; Rettori, C.; Garcia-Adeva, A. J.; Huber, D. L.; Oseroff, S. B.; W Ratcliff, I. I.; Cheong, S. W.; Pagliuso, P. G.; Sarrao, J. L.; Martins, G. B. Magnetic properties of the frustrated antiferromagnetic spinel ZnCr 2 O 4 and the spin-glass Zn1-x CdxCr2O4 (x= 0.05, 0.10). *Phys. Rev. B* **2001**, *64*, No. 024408.
(22) Ostoréro, J.; Mauger, A.; Guillot, M.; Derory, A.; Escorne, M.; Marchand, A. Influence of topological frustration on the magnetic properties of the normal oxyspinel CdFe2O4. *Phys. Rev. B* **1989**, *40*, 391−395, DOI: 10.1103/PhysRevB.40.391.
(23) Morellon, L.; Algarabel, P. A.; Ibarra, M. R.; Blasco, J.; Garcia-Landa, B.; Arnold, Z.; Albertini, F. Magnetic-field-induced structural phase transition in Gd5(Si1.8Ge 2.2). *Phys. Rev. B* **1998**, *58*, R14721−R1724, DOI: 10.1103/PhysRevB.58.R14721.
(24) Choe, W.; Pecharsky, V. K.; Pecharsky, A. O.; Gschneidner, K. A.; Young Jr, V. G.; Miller, G. J. Making and breaking covalent bonds across the magnetic transition in the giant magnetocaloric material Gd5(Si2Ge2). *Phys. Rev. Lett.* **2000**, *84*, 4617−4620, DOI: 10.1103/PhysRevLett.84.4617.
(25) Aliev, O. M.; Agaev, A. B.; Azadaliev, R. A. Synthesis and properties of CdLn2 × 4 (X= S, Se, Te) and CdLn4S7 chalcogenides. *Inorg. Mater.* **1997**, *33*, 1123−1127.
(26) Pandey, S. K. Effect of pressure on the electronic and magnetic properties of CdV2O4: Density functional theory studies. *Phys. Rev. B* **2012**, *86*, No. 085103.
(27) Estrada, F.; Guzmán, E. J.; Navarro, O.; Avignon, M. Curie temperature behavior in half-metallic ferromagnetic double perovskites within the electronic correlation picture. *Phys. Rev. B* **2018**, *97*, No. 195155.
(28) Thompson, S. M. The discovery, development and future of GMR: The Nobel Prize 2007. *J. Phys. D: Appl. Phys.* **2008**, *41*, No. 093001.
(29) Jain, A.; Ong, S. P.; Hautier, G.; Chen, W.; Richards, W. D.; Dacek, S.; Cholia, S.; Gunter, D.; Skinner, D.; Ceder, G.; Persson, K. A. Commentary: The Materials Project: A materials genome approach to accelerating materials innovation. *APL Mater.* **2013**, *1*, No. 011002.
(30) Ding, G.; Wang, J.; Yu, Z. M.; Zhang, Z.; Wang, W.; Wang, X. 2023. Single pair of type-III Weyl points half-metals: $BaNiIO_6$ as an example. *Phys. Rev. Mater.* **2023**, *7*, No. 014202.
(31) Wang, J.; Yuan, H.; Liu, Y.; Wang, X.; Zhang, G. Multiple dimensions of spin-gapless semiconducting states in tetragonal Sr_2CuF_6. *Phys. Rev. B* **2022**, *106*, No. L060407.
(32) de la Mora, P.; Tavizon, G. Rare earth chalcospinels, electronic structure, intermediate-valent, and heavy-fermion character. *J. Solid State Chem.* **2023**, *324*, No. 124056.
(33) Blaha, P.; Schwarz, K.; Madsen, G.; Kvasnicka, D.; Luitz, J. *An Augmented Plane Wave Plus Local Orbital Program for Calculating Crystal Properties*; Vienna University of Technology: Vienna, Austria, 2001.
(34) Wu, Z.; Cohen, E. R. More accurate generalized gradient approximation for solids. *Phys. Rev. B* **2006**, *73*, No. 235116.
(35) Tran, F.; Blaha, P. Accurate band gaps of semiconductors and insulators with a semilocal exchange-correlation potential. *Phys. Rev. Lett.* **2009**, *102*, No. 226401.
(36) Guo, S. D.; Liu, B. G. Improved half-metallic ferromagnetism of transition-metal pnictides and chalcogenides calculated with a modified Becke-Johnson exchange potential. *Euro. Phys. Lett.* **2011**, *93*, No. 47006, DOI: 10.1209/0295-5075/93/47006.
(37) Madsen, G. K.; Singh, D. J. BoltzTraP. A code for calculating band-structure dependent quantities. *Comp. Phys. Commun.* **2006**, *175*, 67−71.
(38) Slack, G. A. *The Thermal Conductivity of Nonmetallic Crystals, Solid state Physics*; Academic Press, 1979; Vol. *34*, pp 1−71.
(39) Jia, T.; Chen, G.; Zhang, Y. Lattice thermal conductivity evaluated using elastic properties. *Phys. Rev. B* **2017**, *95*, No. 155206.
(40) Morelli, D. T.; Jovovic, V.; Heremans, J. P. Intrinsically minimal thermal conductivity in cubici−V−VI_2 semiconductors. *Phys. Rev. Lett.* **2008**, *101*, No. 035901.
(41) Skoug, E. J.; Cain, J. D.; Morelli, D. T. Structural effects on the lattice thermal conductivity of ternary antimony- and bismuth-containing chalcogenide semiconductors. *Appl. Phys. Lett.* **2010**, *96*, No. 181905.
(42) Aroyo, M. I.; Kirov, A.; Capillas, C.; Perez-Mato, J. M.; Wondratschek, H. Bilbao Crystallographic Server II: Representations of crystallographic point groups and space groups″. *Acta Crystallogr.* **2006**, *A62*, 115−128.

https://doi.org/10.1021/acsomega.3c04161
ACS Omega 2023, 8, 40341−40350

(43) Murnaghan, F. D. The compressibility of media under extreme pressures. *Proc. Natl. Acad. Sci. U.S.A* **1944**, *30*, 244−247.
(44) Pokrzywnicki, S.; Czopnik, A. Magnetic Susceptibility of CdTm2S4 Spinel. *Phys. Status. Solidi* **1975**, *70*, K85−K87.
(45) Pokrzywnicki, S.; Pawlak, L.; Czopnik, A. Magnetic susceptibility of Tm2Se3 and CdTm2Se4 compounds. *Physica B+ C* **1977**, *86-88*, 1141−1142.
(46) Reddy, S. D.; Reddy, M. M.; Rao, N. K.; Gunasekhar, K. R.; Reddy, S. P. Structural and morphological properties of thermally evaporated Zn1-xMnxS nano-crystalline films. *J. Opt. Adv. Mater.* **2007**, *9*, 3743−3746.
(47) Ji, X.; Yu, Y.; Ji, J.; Long, J.; Chen, J.; Liu, D. Theoretical studies of the pressure-induced phase transition and elastic properties of BeS. *J. Alloys Compd.* **2015**, *623*, 304−310.
(48) Tvergaard, V.; Hutchinson, J. W. Microcracking in ceramics induced by thermal expansion or elastic anisotropy. *J. Am. Ceram. Soc.* **1988**, *71*, 157−166.
(49) Pugh, S. F. XCII. Relations between the elastic moduli and the plastic properties of polycrystalline pure metals. The London, Edinburgh, and Dublin. *London Edinburgh Philos. Mag. J. Sci.* **1954**, *45*, 823−843, DOI: 10.1080/14786440808520496.
(50) Kleinman, L. Deformation potentials in silicon. I. Uniaxial strain. *Phys. Rev.* **1962**, *128*, 2614−2621.
(51) Kanoun, M. B.; Merad, A. E.; Cibert, J.; Aourag, H.; Merad, G. Properties of strained zinc-blende GaN: first-principlesstudy. *J. Alloys Compd.* **2004**, *366*, 86−93.
(52) Frantsevich, I. N.; Voronov, F. F.; Bokuta, S. A. *Elastic Constants and Elastic Moduli of Metals and Insulators Handbook*; Frantsevich, I. N., Ed.; Naukova Dumka: Kiev, 1983; p 60.
(53) Ou, P.; Wang, J.; Shang, S.; Chen, L.; Du, Y.; Liu, Z. K.; Zheng, F. A first-principles study of structure, elasticity and thermal decomposition of Ti1-xTMxN alloys (TM= Y, Zr, Nb, Hf, and Ta). *Surf. Coat. Technol.* **2015**, *264*, 41−48.
(54) Ali, S.; Rashid, M.; Hassan, M.; Noor, N. A.; Mahmood, Q.; Laref, A.; Haq, B. U. Ab-initio study of electronic, magnetic and thermoelectric behaviors of LiV2O4 and LiCr2O4 using modified Becke-Johson (mBJ) potential. *Phys. B: Condens. Matter* **2018**, *537*, 329−335.
(55) Zanib, M.; Noor, N. A.; Iqbal, M. A.; Mahmood, I.; Mahmood, A.; Ramay, S. M.; Al-Garadi, N. Y.; Uzzaman, T. Density functional theory study of electronic, optical and transport properties of magnesium based MgY2Z4 (Z= S and Se) spinels. *Curr. Appl. Phys.* **2020**, *20*, 1097−1102.
(56) Mahmood, A.; Rashid, M.; Safder, K.; Iqbal, M. W.; Noor, N. A.; Ramay, S. M.; Al-Masry, W.; Al-Garadi, N. Y. Spin-dependent rare-earth-based MgPr2 × 4 (X= S, Se) spinels investigations for spintronic and sustainable energy systems applications. *Res. Phys.* **2021**, *20*, No. 103709, DOI: 10.1016/j.rinp.2020.103709.
(57) Tahir, W.; Mustafa, G. M.; Noor, N. A.; Alay-e-Abbas, S. M.; Mahmood, Q.; Laref, A. Analysis of optoelectronic and trasnport properties of magnesium based MgSc2 × 4 (X= S, Se) spinels for solar cell and energy storage device applications. *Ceram. Int.* **2020**, *46*, 26637−26645.
(58) Kim, K. S.; Han, J. H. Boltzmann transport theory for metal-insulator transitions: Comparison between two and three dimensions. *Eur. Phys. J. B* **2020**, *93*, No. 21, DOI: 10.1140/epjb/e2019-100424-9.
(59) Noor, N. A.; Rashid, M.; Mustafa, G. M.; Mahmood, A.; Al-Masry, W.; Ramay, S. M. Zinc based chalcogenides ZnMn2 × 4 (X= S, Se, Te) as promising spintronic and sustainable energy materials: Ab-initio DFT investigations. *J. Alloys Compd.* **2021**, *856*, No. 157198.
(60) Gandi, A. N.; Alshareef, H. N.; Schwingenschlogl, U. Thermoelectric Performance of the MXenes M2CO2 (M = Ti, Zr, or Hf). *Chem. Mater.* **2016**, *28*, 1647−1652, DOI: 10.1021/acs.chemmater.5b04257.
(61) Tufail, M.; Rahman, A. U.; Gul, B.; Akram, W.; Ullah, H.; Iqbal, M. W.; Ramay, S. M.; Shah, W. H. *Phys. B: Condens. Matter* **2021**, *608*, No. 412789, DOI: 10.1016/j.physb.2020.412789.
(62) Alburaih, H. A. Probing of Ferromagnetism and Electronic transport characteristics of Rare-earth-based $CdEr_2X_4$ (X= S, Se) Spinels for Spintronic and Energy Harvesting Applications. *J. Alloys Compd.* **2021**, *876*, No. 159806.

https://doi.org/10.1021/acsomega.3c04161
ACS Omega 2023, 8, 40341−40350